Progress In Electromagnetics Research, Vol. 119, 477–495, 2011

A CYLINDRICAL SHAPED-REFLECTOR ANTENNA WITH A LINEAR FEED ARRAY FOR SHAPING COMPLEX BEAM PATTERNS

S.-Y. Eom[1], Y.-B. Jung[2,*], S. A. Ganin[3], and A. V. Shishlov[3]

[1]Radio Technology Research Department, Electronics and Telecommunications Research Institute, 138 Gajeong-no, Yuseong-gu, Daejeon, Republic of Korea

[2]Division of Electrics, Electronics and Control Engineering, Hanbat National University, 16-1 Duckmyong-dong, Yusung-gu, Daejeon, Republic of Korea

[3]JSC Radiophyzika, Geroev Panfilovtsev St., 10, Moscow 125480, Russia

Abstract—In this paper, we present a cylindrical shaped-reflector antenna which is spatially fed by an off-set linear feed array to form complex beam patterns. The linear feed array consists of twelve microstrip patch elements and forms a flat-topped beam pattern with a beam-width of $\pm 45^\circ$ in the azimuth plane. The vertical curve on the cylindrical reflector with the linear feed array is shaped to form a cosecant beam pattern within the range of -5° to -25° in the elevation plane. By using the proposed design procedure to form complex beam patterns, a hybrid antenna with a cylindrical reflector aperture of 140 cm $\times$ 50 cm is designed to be operated within the IMT 2000 service band, and a prototype antenna is also fabricated. Its electrical performance is measured and compared with simulation results.

1. INTRODUCTION

Communication is shifting from voice-based wireless services such as cellular phones and PCSs to the IMT-2000 (WCDMA) wireless broadband data service, and the present 2G service bands are expected to gradually converge into the 3G service band. Moreover, the WiBro

Received 29 June 2011, Accepted 8 August 2011, Scheduled 19 August 2011

* Corresponding author: Young-Bae Jung (ybjung@hanbat.ac.kr).

mobile Internet service, for which the upload and download transfer capacity has been technically enhanced to the Mbps level, is thought likely to be extended to a nationwide service in Korea. The base station antennae currently providing such a broadband service generally have a normal beam pattern. In the case of such an antenna beam pattern, the power density near the base station towers is high, but it is insufficient around the sector cell edge. Therefore, efforts have been made to develop various techniques to guarantee the quality of service (QoS) within the sector cell area, such as transmission power control and new service scheduling. The wide range of the transmission power control requires a relatively stronger power amplifier, consumes more power, and decreases the reliability of the transmission system.

This paper is aimed at overcoming such problems in terms of the base station antenna (BSA) design technology. To efficiently use the power of a given base station system as shown in Figure 1, it is necessary to provide uniform power flux density (PFD) for the subscribers within the sector cell area.

For this to happen, the antenna should form the complex beam patterns of a flat-topped beam pattern (FBP) in the azimuth plane and a cosecant beam pattern (CBP) in the elevation plane. That is, the FBP is flat at the center and is steeply sloped at its edge, and the radiation pattern in the elevation plane forms a cosecant envelope for the power flux density to be uniform according to the elevation service distance.

The technology for controlling the output power of a linear power amplifier incorporates the concept of active power control, while

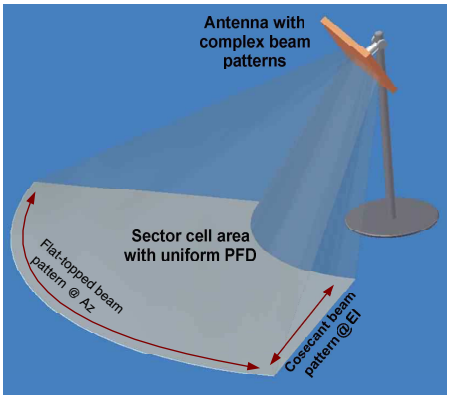

Figure 1. Sector cell area with uniform PFD covered by complex beam patterns.

the technology for shaping antenna beam patterns incorporates the concept of passive power control. This can transfer the power density from the affluent area to the insufficient area to improve the power efficiency within the sector cell through antenna beam pattern shaping. Such antenna technology has the following merits.

- It reduces irregular damping in the sector cell area and improves the deterioration of data quality that occurs at a cell's edge.
- It greatly reduces active power control between the base station and terminals.
- It saves on system investment costs by extending the sector cell range.
- It enhances the subscribers' satisfaction by increasing the residual time of the terminal batteries.

We can design and analyze a complex shaping beam pattern by using the linear or planar array antenna design [1–6], the double-shaping reflector design [7], and various other antenna structures, such as hybrid antenna design [8, 9]. The hybrid antenna refers to an antenna consisting of a reflector and a feed array. In this paper, we suggest a hybrid antenna structure consisting of a cylindrical shaping reflector and a linear feed array (LFA) to efficiently form the FBP in the azimuth plane and the CBP in the elevation plane. This is a method of forming the aperture field of a reflector antenna by spatial radiation of the LFA. The FBP is formed only by the LFA. The electromagnetic wave radiated from the LFA is just reflected by the cylindrical reflector to a free space. The CBP in the elevation plane is formed by the one-dimensional surface shaping of the cylindrical reflector. The complex beam pattern conditions of the antenna, which is the subject of this paper, have a FBP characteristic of $\pm 45^\circ$ at the 3 dB level in the azimuth plane and a cosecant beam envelope characteristic within the range of -5° to -25° in the elevation plane.

In addition, the operating frequency band is assumed to be the IMT-2000 service band (1.92 GHz to 2.17 GHz), and the polarization characteristic is assumed to be linear vertical polarization.

2. PROPOSED ANTENNA STRUCTURE AND DESIGN PROCEDURE

An off-set hybrid antenna structure is suggested to form the FBP in the azimuth plane and the cosecant beam pattern in the elevation plane, as shown in Figure 2.

The design variables D_x, and D_y in Figure 2 indicate the size of the reflector aperture in the x and y axial directions, F indicates the

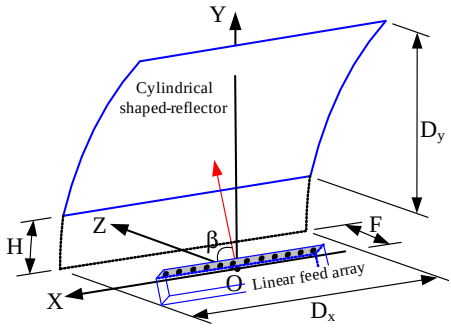

Figure 2. Proposed antenna structure.

focal length, H the off-set displacement from the z axis, and β the angle elevated from the XOZ plane of the LFA.

The design procedure followed to ensure that the hybrid antenna forms different complex beam patterns in the azimuth and elevation plane is shown in Figure 3.

As shown in Figure 3, the FBP in the azimuth plane is formed by the LFA, and the pattern synthesis method of optimizing the phase distribution under a given amplitude distribution is used to obtain the aperture amplitude and phase distribution data required by the LFA [10, 11]. The LFA consists of twelve radiating elements and the array feed network. The design is described in detail in Section 3.1. On the other side, the CBP in the elevation plane is formed through the cylindrical reflector's one-dimensional shaping. The cylindrical reflector means that the z coordinates on the XOZ plane are all equal as shown in Figure 4.

The shaping of the cylindrical reflector begins with a parabola curve on the YOZ plane, and can be expressed as

$$z = F - \frac{y^2}{4F} \tag{1}$$

The surface of the reflector is determined by a one-dimensional spline in the rectangular lattice. That is, the central nodes of the lattice are fixed and the surrounding nodes move up and down along the z axis, which form the reflector surface design vector $\boldsymbol{\mu} = [z_1, z_2, \ldots, z_L]^{\mathrm{T}}$. Such surface design vectors are calculated through the reflector optimum shaping process based on physical optics. The antenna radiation pattern is given as in [7, 9] as

$$G(\mathbf{p}, \boldsymbol{\mu}) = \begin{bmatrix} G(p_1, \boldsymbol{\mu}) \\ \vdots \\ G(p_n, \boldsymbol{\mu}) \end{bmatrix} \tag{2}$$

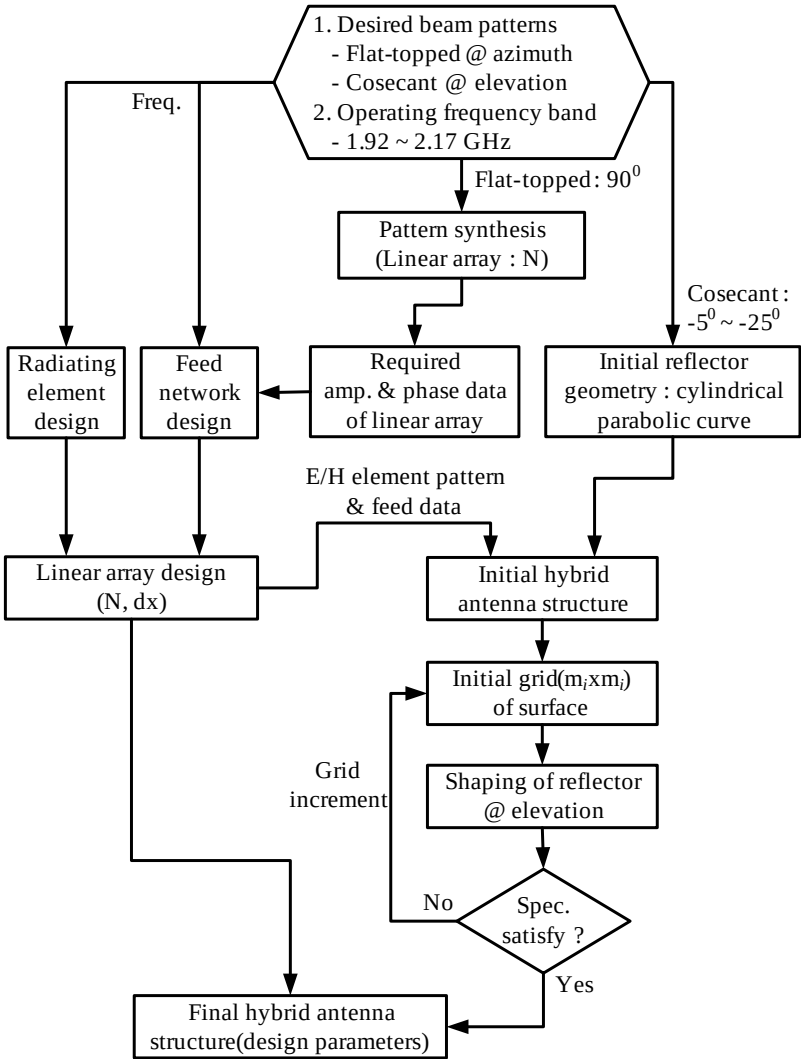

Figure 3. Design procedure for shaping a complex beam pattern.

where $\mathbf{p} = [p_1, p_2, \ldots, p_n]^{\mathrm{T}}$ is the set of observation points in the far-field elevation pattern. The reflector shaping algorithm minimizes the distance between the desired radiation pattern and the actual radiation pattern, as shown in the following expression:

$$\min_{\boldsymbol{\mu}} \|G(\mathbf{p}, \boldsymbol{\mu}) - G_d(\mathbf{p})\|^2 = \min_{\boldsymbol{\mu}} \left\{ \sum_{i=1}^{n} [G(p_i, \boldsymbol{\mu}) - G_d(p_i)]^2 \right\} \quad (3)$$

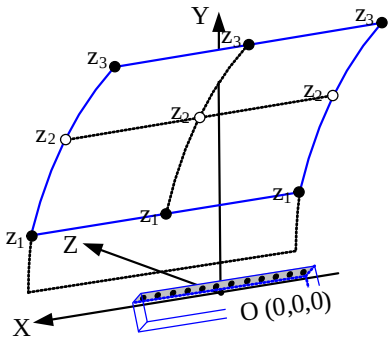

Figure 4. Cylindrical reflector's one-dimensional shaping. (3×3 rectangular lattice).

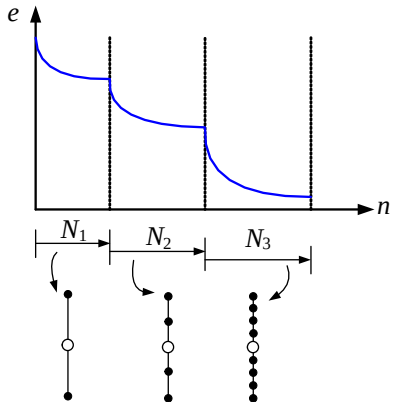

Figure 5. Optimization design process according to extension of the lattice.

where $G(\mathbf{p}, \boldsymbol{\mu})$ and $G_d(\mathbf{p})$ represent the actual radiation pattern and the desired (cosecant) radiation pattern, respectively.

With respect to the given design vectors, the convergence of the pattern error e of the desired radiation pattern and the actual radiation pattern according to the number n of the radiation pattern repetition calculations is shown in Figure 5. In Figure 5, the error sharply declines first and is then rapidly converged to the minimum value ($N_1 < N_2 < N_3$). Therefore, in the reflector shaping algorithm, the optimization process for reducing the design calculations is important. In other words, as the calculation of a high number of lattice nodes takes up a relatively large amount of time, it is more efficient to calculate the pattern error by the minimum number of lattices and, when the pattern error comes into the given error range, to extend the lattice number again and then calculate the minimum pattern error.

If the distance between the fixed node and the adjacent nodes in the y axis direction is less than a wavelength, no more extension of the lattice is required and the optimization process ends.

3. HYBRID ANTENNA DESIGN

3.1. Linear Feed Array Design

The single radiating element of the LFA is shown in Figure 6. This is the broadband structure [12] that was chosen by taking into account the operating band. As the space between the epoxy substrate (FR-4,

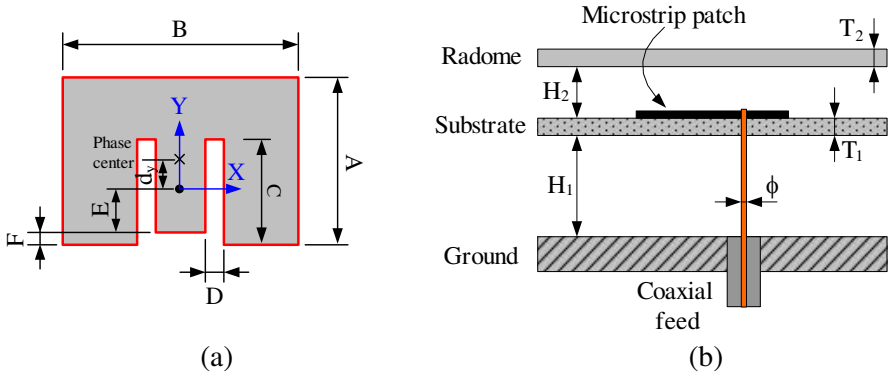

Figure 6. Radiating element excited by coaxial line: (a) Geometry of the patch ($A = 50\,\text{mm}$, $B = 70.4\,\text{mm}$, $C = 30.9\,\text{mm}$, $D = 5.2\,\text{mm}$, $E = 12.0\,\text{mm}$, $F = 3.5\,\text{mm}$). (b) Cross-section view ($H_1 = 9.4\,\text{mm}$ (air), $H_2 = 1.0\,\text{mm}$ (air), $T_1 = 1.0\,\text{mm}$, $T_2 = 1.0\,\text{mm}$, $\phi = 0.67\,\text{mm}$).

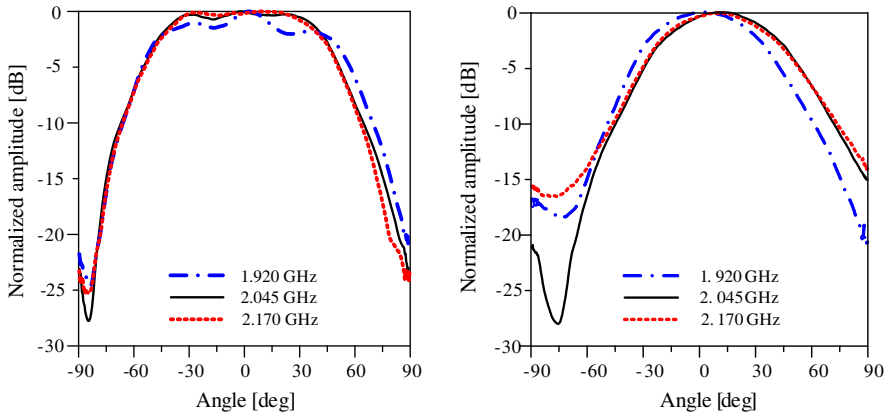

Figure 7. Measured radiation patterns of the single radiating element.

$\varepsilon_r = 4.4$), the radome substrate (polystyrene, $\varepsilon_r = 2.6$), and the base ground should be filled with air, an auxiliary separating material is used to support them.

The LFA is arranged linearly in the azimuth direction (x-axis direction) with twelve radiating elements as shown in Figure 6. As the distance between the array elements is 8.1 cm ($0.55\lambda_o$), the length of the entire LFA is about 100 cm, including the guard on the edge. The measured radiation pattern of the designed and fabricated single

radiating element is shown in Figure 7. The radiating element used for measurement here, in which the mutual coupling characteristics with adjacent elements are reflected, is located in the middle of the 5 radiating elements, and the mutual coupling amount between the elements is below −20 dB.

The amplitude and phase distribution required at the LFA aperture to form an FBP with a beam-width of ±45° is shown in Figure 8. It can be obtained through the pattern synthesis that has considered the given array spacing and the properties of the single radiating elements described in this paper.

To realize the LFA aperture distribution shown in Figure 8, the feed network was designed for the LFA, as shown in Figure 9. The feed network is bilaterally symmetrical and has twelve output ports for one input. The internal network consists of a Wilkinson power divider

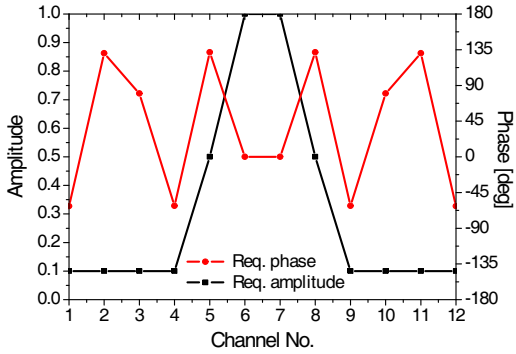

Figure 8. Amplitude and phase distributions required in the LFA.

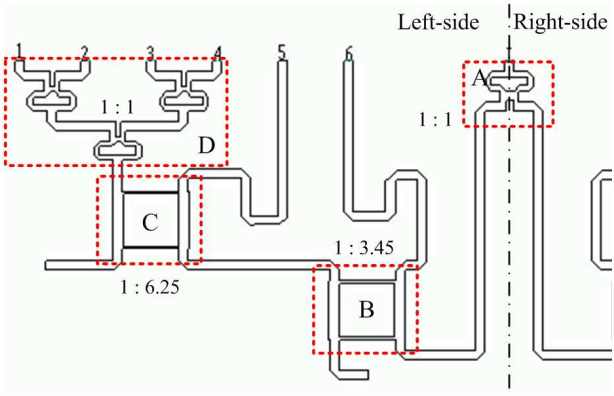

Figure 9. Feed network for the LFA (half).

(A) with a 1 : 1 power ratio, two 90° branch-line couplers (B) with a 1 : 3.45 power ratio, two 90° branch-line couplers (C) with a 1 : 6.25 power ratio, and two 4-way power dividers (D) comprising three 1 : 1 Wilkinson power dividers in order to produce the required amplitude and phase distributions. The connection between the input ports of the twelve radiating elements and the output ports of the feed network is made by coaxial cables. The measured amplitude and phase data are shown in Tables 1 and 2, respectively.

From the comparison of the required and measured amplitude and the phase data shown in Tables 1 and 2, the amplitude error is below 0.03 (0.3 dB) in the center frequency and ±24.2° on the edge of the operating band. The fact that the amplitude error is larger on the edge than at the center is due to the frequency-phase dispersion effect of the transmission lines used for the feed network and coaxial cable.

The measured FBPs of the LFA prototype within the operating band are shown in Figure 10. They show ripple characteristics below ±2.1 dB in the flat-topped beam-width. This can be resolved by more accurately implementing the amplitude and phase distribution of the feed network. From Figure 10, it can be known that the measured 3 dB flat-topped beam-widths of the antenna prototype are 97.4°, 88.1°, and 83.1° at $f = 1.92$ GHz, $f = 2.045$ GHz, and $f = 2.17$ GHz, respectively, and that the side lobe level is less than −22.1 dB within the operating band.

Table 1. Amplitude data measured in the feed network.

Channel No.	Required amplitude	Measured amplitude		
		1.92 GHz	2.045 GHz	2.17 GHz
1	0.1	0.11	0.11	0.11
2	0.1	0.11	0.10	0.10
3	0.1	0.11	0.09	0.10
4	0.1	0.11	0.10	0.10
5	0.5	0.50	0.50	0.50
6	1.0	0.97	1.00	0.98
7	1.0	0.97	0.99	0.97
8	0.5	0.50	0.50	0.49
9	0.1	0.11	0.10	0.10
10	0.1	0.11	0.09	0.10
11	0.1	0.11	0.10	0.10
12	0.1	0.11	0.11	0.11

Table 2. Phase data measured in the feed network.

Channel No.	Required Amplitude [deg]	Measured amplitude [deg] 1.92 GHz	2.045 GHz	2.17 GHz
1	−62.20	−47.00	−60.00	−81.00
2	130.50	141.00	138.00	132.00
3	79.70	89.00	80.00	71.00
4	−61.80	−44.00	−62.00	−81.00
5	131.80	146.00	137.00	125.00
6	0.00	−4.00	1.00	−0.40
7	0.00	−6.00	−0.60	−2.20
8	131.80	144.00	135.00	124.00
9	−61.80	−41.00	−58.00	−75.00
10	79.70	86.00	77.00	68.00
11	130.50	133.00	131.00	126.00
12	−62.20	−38.00	−57.00	−74.00

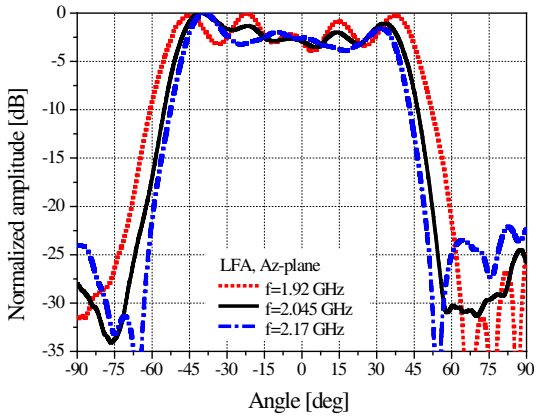

Figure 10. Measured flat-topped beam patterns of LFA.

3.2. Cylindrical Reflector Design

In the design of the complex beam pattern proposed in this paper, the size of the cylindrical reflector depends on the size of the LFA forming the FBP in the azimuth plane (or H-plane) and on the required conditions (cosecant envelop range and error) of the CBP formed in the elevation plane (or E-plane). The horizontal length of the reflector to reduce the spatial spillover loss of the LFA and side lobe level can

initially be chosen by expression (4) with the length (d_o) of the LFA and a flat-topped beam-width, as shown in Figure 11. Therefore, to reduce the horizontal length of the reflector, the focal length should be shortened. However, the exact horizontal length of the reflector is determined through a physical optics-based simulation.

$$D_x = d_o + 2 \cdot F \cdot \tan\left(\frac{\theta_{FT}}{2}\right) \tag{4}$$

where d_o is the length of the feed array, F is the focal length, and θ_{FT} is the flat-topped beam-width.

The phase center of the LFA in the hybrid antenna should be situated along the focal length of the reflector. The single radiating element comprising the LFA is asymmetrical on the E-plane (y-axis direction) as shown in Figure 6(a), so the phase center of the feed array must be accurately predicted. Figure 12 illustrates the phase patterns of the LFA on the E-plane. The phase pattern is almost constant when offset by 1 mm from the origin, that is, when $d_y = 1.0$ mm. This point corresponds to the center of the radiating patch element.

The amplitude envelope of the CBP in the elevation plane can be defined as

$$E_{el}(\theta) = \frac{\sin(\theta_o)}{\sin(\theta_o - \theta)}, \quad \theta \in [-\theta_m, 0] \tag{5}$$

where $E_{el}(\theta)$ is the elevation amplitude pattern, θ_o is the maximum gain oriented angle, and θ_m is the maximum cosecant angle. In this paper, we consider that $\theta_o = 5^\circ$ and $\theta_m = 25^\circ$. According to

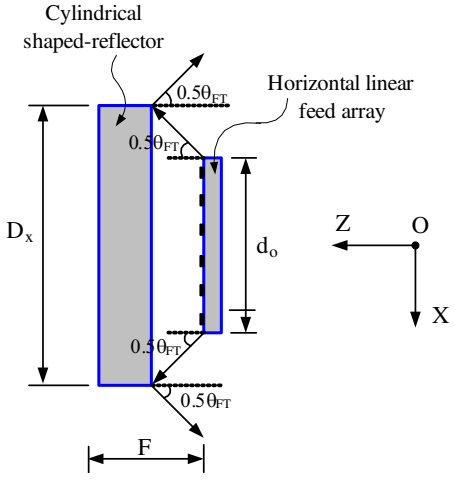

Figure 11. Initial choice of the reflector horizontal length.

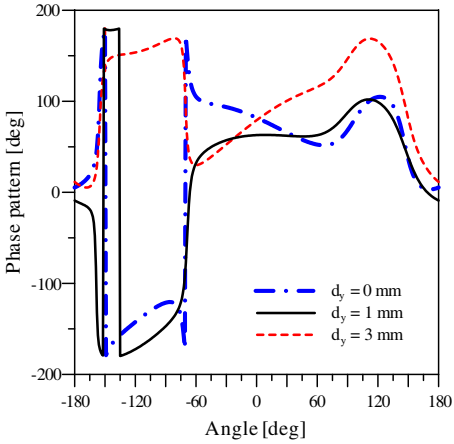

Figure 12. Phase pattern of the LFA on the E-plane.

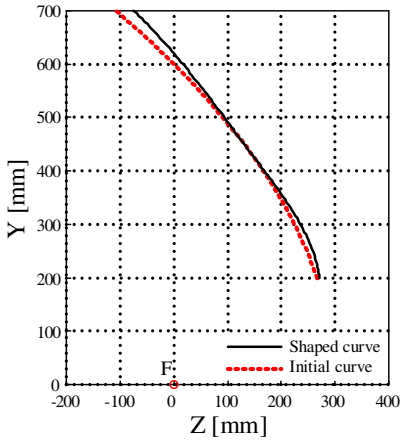

Figure 13. Cross-section (x-axis) of the cylindrical reflector.

the requirements of the CBP, the vertical length of the reflector is determined, and the shaping of the reflector is different. The geometric design parameters of the reflector, such as D_y, H, and F in Figure 2, are determined so that no blocking effect is caused by the LFA and so that the beam oriented angle of the LFA towards the reflector is met.

The input/initial data used for the cylindrical reflector shaping simulation to provide complex beam patterns is summarized in Table 3, and the x-axis cross section of the cylindrical reflector for manufacturing an antenna prototype is shown in Figure 13.

3.3. Antenna Prototype Fabrication and Test Results

A prototype of the hybrid antenna used to shape the complex beam patterns was fabricated to test the electrical performance. The dimensions of the fabricated antenna are 140 cm (horizontal) by 50 cm (vertical). To manufacture the reflector, thin metal shaping frames were made in the elevation direction and arranged at certain intervals. They were then covered with a wide, thin metal panel with the bolts screwed. As the operating band is relatively low (2 GHz), this method both reduces the manufacturing cost and greatly decreases the total weight of the antenna. Figure 14 is a photograph of the antenna prototype installed on an anechoic chamber tower to measure the radiation patterns.

Figure 15 shows the parts comprising the LFA. Figure 15(a) shows the radiating array board, and Figure 15(b) shows the feed network

Table 3. Input/initial data for cylindrical reflector shaping simulation.

Items		Input/initial data
Linear feed array	Radiating element pattern	Simulated E-pattern data
		Simulated H-pattern data
	Aperture amplitude and phase data	Required amplitude data in Table 1
		Required amplitude data in Table 2
	Array spacing	8.06 cm (0.55λo)
	Number of array elements	12
Cylindrical reflector geometric structure	D_x	140 cm
	D_y	50 cm
	H	20 cm
	F	30 cm
	β	60°

Figure 14. Photo of the antenna prototype installed on an anechoic chamber tower.

that provides the required amplitude and phase data of the LFA aperture. The antenna phase is corrected by adjusting the length of the coaxial cables necessary for connecting between the output ports of the feed network and the input ports of the radiating elements. The amplitude and phase data measurements within the operating band are shown in Tables 1 and 2.

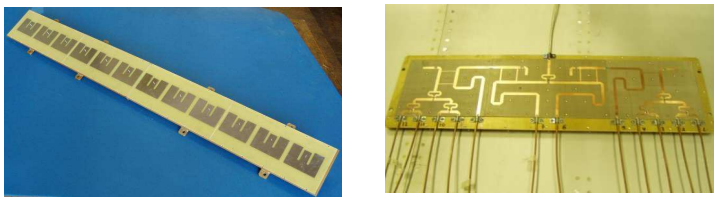

(a) (b)

Figure 15. Fabricated LFA prototype: (a) radiating element array board. (b) Feed network board with the coaxial cables.

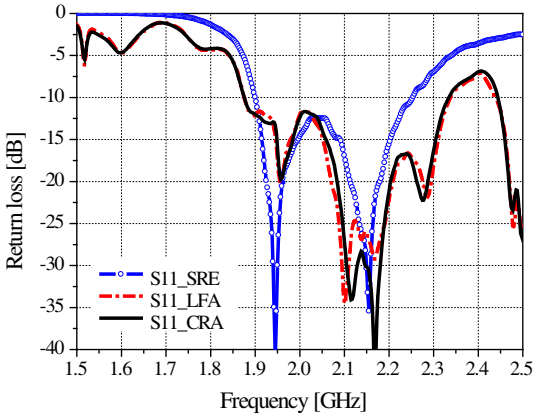

Figure 16. Measured input return losses.

The measured input return losses of the hybrid antenna prototype are shown in Figure 16 along with the single radiating element and the LFA. All of them show a similar form of less than -12 dB within the operating band.

The measured radiation patterns of the hybrid antenna prototype within the operating band are shown in Figures 17 and 18 along with the simulated radiation patterns. Figure 17 shows the FBP characteristics in the azimuth plane by frequency, and Figure 18 shows the CBP characteristics in the elevation plane.

Figure 17 shows that the measured FBPs of the hybrid antenna are relatively consistent compared with the simulated ones within the operating band. They show ripple characteristics below ± 1.5 dB in the flat-topped beam-width, which is attributable to the ripple characteristics of the LFA. This can be resolved by more accurately implementing the amplitude and phase characteristics of the feed array

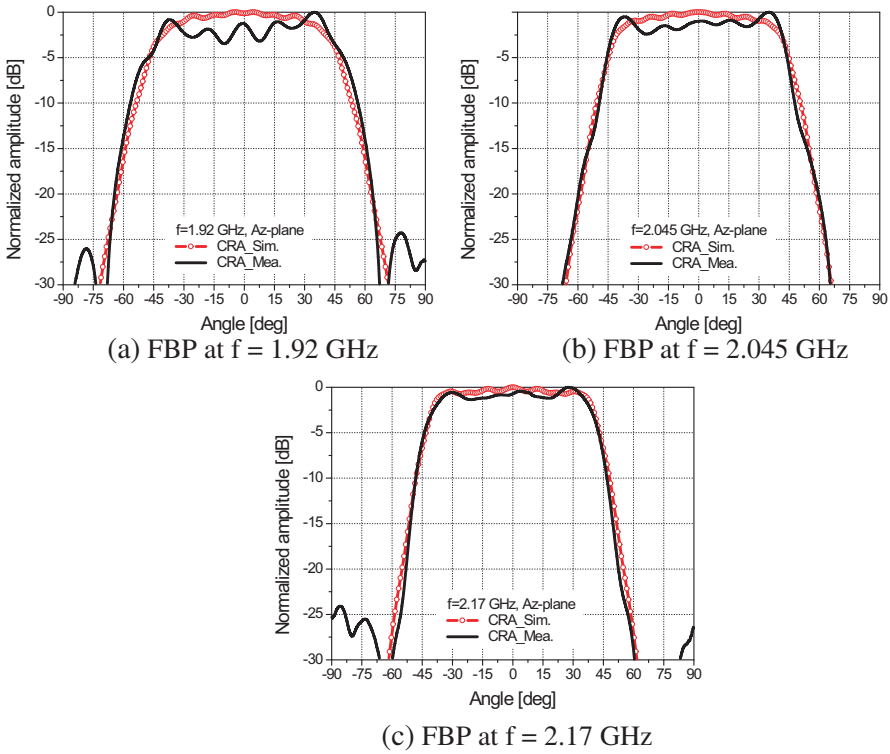

(a) FBP at f = 1.92 GHz

(b) FBP at f = 2.045 GHz

(c) FBP at f = 2.17 GHz

Figure 17. Measured flat-topped beam patterns of CRA.

aperture. From Figure 17, it can be known that the measured 3 dB flat-topped beam-widths of the antenna prototype are 86.6°, 85.6°, and 80.4° at $f = 1.92$ GHz, $f = 2.045$ GHz, and $f = 2.17$ GHz, respectively, and that the side lobe level is below -24.1 dB within the operating band.

In addition, Figure 18 shows that the measured elevation patterns of the hybrid antenna are consistent with the simulated ones within the cosecant beam range of $-5°$ to $-25°$, but the side lobe characteristics are relatively inconsistent. One reason for this is the electromagnetic wave scattering impact caused by the metal supporting device connecting the cylindrical reflector and the LFA. This was confirmed by an experiment which showed that the side lobe level went down as it was covered with absorber materials. Therefore, it is necessary to consider the spatial feed area of the LFA in designing the supporting device to ensure that the supporting device does not affect the electrical performance of the antenna. Another explanation is based on the

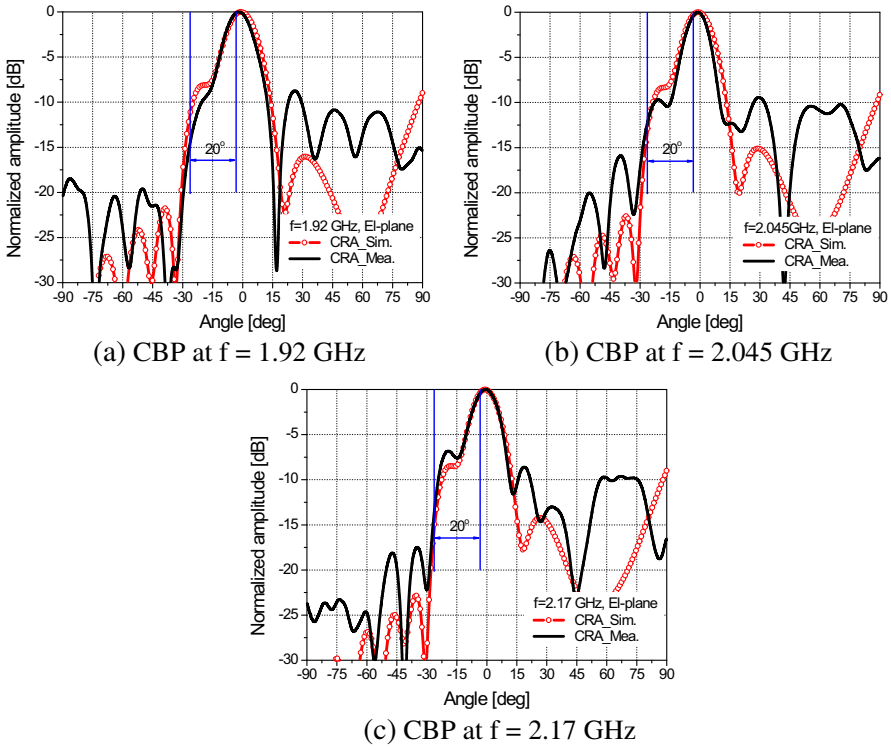

(a) CBP at f = 1.92 GHz (b) CBP at f = 2.045 GHz

(c) CBP at f = 2.17 GHz

Figure 18. Measured cosecant beam patterns of CRA.

assumption that the radiation pattern in the reflector design simulation is mostly determined by the reflector.

This assumption is effective when the reflector antenna has much greater directivity than the LFA. In general, the antenna directivity can be expressed by the horizontal pattern directivity multiplied by the vertical pattern directivity. In this paper, the horizontal directivity of the reflector and that of the LFA are almost equal, but their vertical directivity differs by one order. Therefore, the electromagnetic wave scattering of the relatively thin reflector in the vertical direction seems to be the cause of the great difference in the characteristics of the elevation side lobe. In the measured cosecant patterns, the beam parts within the range of 0° to 90° face upwards, and those within the range of 0° to −90° face downwards, so the latter are the more important characteristics. Therefore, as seen in Figure 18, the side lobe levels between −25° to −90° can be measured below −15.9 dB within the operating band. Also, through the pattern measurements,

Table 4. Measured gain of the antenna prototype.

Frequency	Simulated gain [dBi]	Measured gain [dBi]	Gain deviation [dB]
1.920 GHz	10.4	8.1	−2.3
2.045 GHz	11.3	10.1	−1.2
2.170 GHz	11.2	10.9	−0.3

the cross polarization characteristics within the operating band are below −23.2 dB in the bore-site direction, and range between −12 to −16 dB in the service sector area. The antenna gains of the antenna prototype were measured by the frequency sweep, calibrating relatively the measured levels with the reference levels of the standard horn antenna. The gain measurements as compared with the simulated gain are summarized in Table 4.

The gain deviation between the measured and simulated gains was rather large at 1.92 GHz and 2.045 GHz because the maximum gain in the azimuth plane was positioned in a different direction due to the ripple characteristics of the FBP. The gains measured in the bore-site direction were −1.3 dB, −1.0 dB, −0.7 dB, smaller than the maximum value at 1.92 GHz, 2.045 GHz, and 2.17 GHz, respectively. Also, the maximum gain of the CBP, offset by about −2° to −3°, was about −0.3 dB smaller than the maximum value.

4. CONCLUSION

A hybrid cylindrical reflector antenna fed by the LFA to shape complex beam patterns was presented. The antenna, which is designed in the IMT-2000 band can shape the FBP with a beam-width of ±45° in the azimuth plane and can simultaneously form the CBP within the range of −5° to −25°.

A hybrid antenna prototype with a cylindrical reflector aperture of 14 cm × 50 was designed using the design procedure proposed in this paper, and a prototype antenna was fabricated and tested. The measured radiation patterns showed good agreement with the simulated patterns.

Antenna pattern synthesis is a kind of passive power control that is used to manage the power flux density within the sector cell area. The complex beam patterns giving uniform power density within the cell area present numerous advantages in terms of wireless mobile communication Therefore, with the convergence of wireless communication services, it will be necessary to conduct research on

the pattern synthesis technology of the base station antenna described in this paper, for the efficient use of the output power of the base station system in future broadband services.

REFERENCES

1. Lee, G. and M. Masound, "Design of a base station antenna with a sharp roll-off sector pattern," *IEEE Int. Antennas and Propagation Symp.*, Vol. 34, 1602–1605, Jul. 1996.
2. Matsumoto, K., E. T. Rahardjo, and M. Haneishi, "Beam shaping using a micro-strip array antenna," *Proceedings of Conference "Journees Internationales de Nice sur les Antennes," Jina '94*, 670–673, Nice, France, Nov. 1994.
3. Eom, S. Y., C. S. Pyo, S. I. Jeon, S. A. Ganin, A. Shishlov, A. V. Shubov, A. G. Tscherbenkov, and V. Ya, "Research of a planar array antenna with a flat-topped radiation pattern for perspective base stations of mobile communication," *Antennas*, Vol. 92, No. 1, 30–38, 2005 (in Russian).
4. Skobelev, S. P., "Analysis and synthesis of array antenna with element flat-topped patterns," *Radiotechnika*, No. 10, 44–47, 1990 (in Russian).
5. Chou, H.-T., K.-L. Hung, and C.-Y. Chen, "Utilization of a Yagi antenna director array to synthesize a shaped radiation pattern for optimum coverage in wireless communications," *Journal of Electromagnetic Waves and Applications*, Vol. 23, No. 7, 851–861, 2009.
6. Alvarez Folgueiras, M., J. A. Rodriguez Gonzalez, and F. J. Ares-Pena, "Analysis of Tolerance among the solutions to shaped-beam synthesis problems," *Journal of Electromagnetic Waves and Applications*, Vol. 24, No. 10, 1341–1352, 2010.
7. Reutov, A. S. and A. V. Shishlov, "Features of the stepwise contour beam reflector antenna synthesis using cubic spline representation of reflector surface," *Electromagnetic Waves and Electric Systems*, No. 2, 4–14, Moscow, 2003.
8. Skobelev, S. P., "Parabolic cylindrical antenna with linear array forming flat-topped element radiation patterns," *Radiotechnika*, No. 6, 42–48, 2004 (in Russian).
9. Reutov, A. S. and A. V. Shishlov, "Focuser-based hybrid antennas for one-dimensional beam steering," *Proceedings of the 2000 IEEE International Conference on Phased Array Systems and Technology*, 411–414, Dana Point, California, 2000.

10. Kondrat'ev, A. S. and A. D. Khzmalyan, "Phase-only synthesis of antenna arrays for a given amplitude radiation pattern," *Journal of Communications Technology and Electronics*, Vol. 41, No. 10, 1996.
11. Li, G., S. Yang, M. Huang, and Z.-P. Nie, "Sidelobe suppression in time modulated linear arrays with unequal element spacing," *Journal of Electromagnetic Waves and Applications*, Vol. 24, No. 5–6, 775–783, 2010.
12. Yu, G., K. P. Esselle, and T. S. Bird, "Broadband E-shaped patch antenna for 5–6 GHz wireless computer network," *Proceedings of the IEEE Int. Antennas and Propagation Symp.*, Vol. 2, 942–945, Jun. 2003.